Continental constriction and oceanic ice-cover thickness in a Snowball-Earth scenario

Eli Tziperman,[1] Dorian S. Abbot,[2] Yosef Ashkenazy,[3] Hezi Gildor,[4] David Pollard,[5] Christian G. Schoof,[6] and Daniel P. Schrag[1]

[1] Ice flow over a Snowball ocean was shown in recent years to be capable of very effectively homogenizing ice thickness globally. Previous studies all used local or one-dimensional global (latitude-only) models, formulated in a way that is difficult to extend to two-dimensional global configuration. This paper uses a two-dimensional global ice flow model to study the effects of continental constriction on ice flow and ice thickness in a Snowball-Earth scenario using reconstructed Neoproterozoic landmass configuration. Numerical simulations and scaling arguments are used to show that various configurations of continents and marginal seas which are not represented by one dimensional models lead to large ice thickness variations, including narrow areas between sub-continents and marginal seas whose entrance is constricted. This study ignores many known important factors such as thermodynamic, optical effects, dust and dust transport, and is therefore meant as a process study focusing on one specific effect, rather than a realistic simulation of Neoproterozoic ice thickness. The model formulation developed here generalizes and extends previous results in several ways, including the introduction of corrections due to spherical coordinates and lateral geometry. This study is therefore a step toward coupling Snowball ice flow models to general circulation ocean and atmospheric models and allowing a more quantitative simulation of Neoproterozoic Snowball ice thickness.

1. Introduction

[2] Between 750 and 580 million years (Myr) ago, during the Neoproterozoic era, Earth experienced multiple ice ages, some of which deposited glaciogenic sediments in equatorial seas indicating possible global ice cover [*Harland*, 1964; *Kirschvink*, 1992; *Hoffman et al.*, 1998]. Understanding these events is an interesting challenge to our knowledge of climate dynamics. Some of the related issues and controversies are described in a recent review by *Pierrehumbert et al.* [2011].

[3] The flow of ice over the ocean in a Snowball Earth scenario has received significant attention over the past few years. It was demonstrated by *Goodman and Pierrehumbert* [2003], that ice flow effectively homogenizes ice thickness in a Snowball Earth scenario. Ice thickness, in turn, plays a potentially important role in the question of the survival of photosynthetic life during a Snowball event [*Hoffman and Schrag*, 2002; *Pollard and Kasting*, 2005; *McKay*, 2000; *Campbell et al.*, 2011], and an ice cover of more than tens of meters could be too thick for photosynthesis [*McKay*, 2000].

[4] Related work has so far dealt with the consequences of ice flow [*Goodman and Pierrehumbert*, 2003], with the optical properties of ice [*McKay*, 2000; *Warren et al.*, 2002], with the effect of different optical properties of frozen seawater vs. accumulated snow [*Pollard and Kasting*, 2005, 2006; *Warren and Brandt*, 2006; *Goodman*, 2006], with the role of dynamic vs. thermodynamic sea ice [*Lewis et al.*, 2007], and with dust accumulation over the Snowball ice cover [*Abbot and Pierrehumbert*, 2010; *Le Hir et al.*, 2010] and dust transport [*Li and Pierrehumbert*, 2011].

[5] *Warren et al.* [2002] and *Pollard and Kasting* [2005] suggested that constricted marginal seas may lead to large

[1] Department of Earth and Planetary Sciences and School of Engineering and Applied Sciences, Cambridge, Massachusetts, USA.

[2] Department of Geophysical Sciences, University of Chicago, Chicago, Illinois, USA.

[3] Department of Solar Energy and Environmental Physics, BIDR, Ben-Gurion University, Midreshet Ben-Gurion, Israel.

[4] Fredy and Nadine Herrmann Institute of Earth Sciences, Hebrew University of Jerusalem, Jerusalem, Israel.

[5] Department of Geosciences, Earth and Environmental Systems Institute, Pennsylvania State University, University Park, Pennsylvania, USA.

[6] Department of Earth and Ocean Sciences, University of British Columbia, Vancouver, British Columbia, Canada.

Corresponding author: E. Tziperman, Department of Earth and Planetary Sciences, Harvard University, 20 Oxford St., Cambridge, MA 02138, USA. (eli@eps.harvard.edu)

ice thickness variations because the ice flow into the sea is limited by friction with the sidewalls of the leading passage, and may not be able to balance the ablation/melting within the sea. In a recent work, especially relevant to the work presented here, *Campbell et al.* [2011] considered the invasion of an elongated rectangular-shaped marginal sea by ice flow, under the influence of friction by the sidewalls of the sea. They derived a formula for the invasion length based on an analytic solution of *Nye* [1965].

[6] All calculations of Snowball ice flow that have so far been carried out used either one-dimensional (in latitude) global models, or an idealized local rectangular marginal sea. Furthermore, the formulation of global one dimensional (latitude only) models was based on a formula for ice shelf deformation rate [*Weertman*, 1957], which, unfortunately, cannot be extended to two dimensions (longitude and latitude).

[7] This paper has two main objectives. The first objective is to study the ice flow on a sphere in the presence of continents, and the possibility of large ice thickness variations developing due to the existence of constricted seas. We show numerical solutions based on reconstructed continental configuration for the Neoproterozoic, as well as scaling relationships for ice thickness variations. We derive scaling relationships for both a global continent-free ocean, and for a constricted sea with a channel connecting it to the ocean.

[8] Our second objective is to formulate the ice flow problem on a sphere, including both horizontal dimensions. To do this, we introduce several novel aspects and introduce physical processes and mathematical terms so far neglected in the Snowball literature. Importantly, we derive the equations directly from the Stokes equations. This allows the formulation of a two-dimensional horizontal flow problem, which is not possible using the approach of pioneering studies of Snowball ice flow [*Goodman and Pierrehumbert*, 2003; *Pollard and Kasting*, 2005] because they started from the ice shelf strain rate formula of *Weertman* [1957]. In particular, we employ the ice shelf momentum budget of *Morland* [1987] [see also *MacAyeal and Barcilon*, 1988; *MacAyeal*, 1989, 1997], as well as spherical coordinates, and show that both of these factors lead to additional terms even in a one-dimensional formulation.

[9] Many factors are now known to play a role in setting ice thickness on a Snowball Earth, and some of them (ice optical properties, different ice sources, dust and dust transport) have been studied in the papers mentioned above. In this paper, we focus on the effects of the ice flow and its interaction with continental configuration, and ignore, for now, all other feedbacks. This has the advantage of allowing us to isolate and carefully study the related flow dynamics, but necessarily makes this study idealized and over-simplified. We feel this is a useful approach, yet emphasize that as a result we do not expect the numerical values of the ice thickness calculated here to be a reliable quantitative predictor of Snowball ice thickness. This work should therefore be viewed as a process study rather than an attempt at a realistic Snowball simulation. In particular, we assume that the ocean is entirely covered with thick ice (termed "sea glaciers" by *Warren et al.* [2002]), and our results cannot be used to confirm or reject the possibility of ice-free conditions or thin ice developing in the tropics as suggested in some previous works [e.g., *Chandler and Sohl*,

2000; *Hyde et al.*, 2000; *Pollard and Kasting*, 2005; *Liu and Peltier*, 2010; *Abbot et al.*, 2011].

[10] In the following sections we present an outline derivation of the model equations (section 2). These equations are a simple extension to spherical coordinates of well-known ice shelf equations used for a long time in glaciology [*Morland*, 1987; *MacAyeal*, 1997]. We then show the model results (section 3), derive scaling laws for ice thickness in an axisymmetric global case without continents and in the case of a constricted sea (section 4), and conclude in section 5. The appendices present a detailed derivation of the model equations.

2. The Model: Two-Dimensional Ice Shelf Flow on a Sphere

[11] We provide an outline of the model derivation here, with full details given in Appendix A. Let the coordinates (longitude, co-latitude, vertical) be denoted by (ϕ, θ, z) and the corresponding velocities be (u, v, w). The momentum equations are,

$$
\begin{aligned}
0 &= -\frac{1}{r\sin\theta}\partial_\phi p + (\nabla \cdot \tau) \cdot \hat{\mathbf{e}}_\phi \\
0 &= -\frac{1}{r}\partial_\theta p + (\nabla \cdot \tau) \cdot \hat{\mathbf{e}}_\theta \\
0 &= -\partial_z p - g\rho_I + (\nabla \cdot \tau) \cdot \hat{\mathbf{e}}_z,
\end{aligned}
\tag{1}
$$

where r is the Earth radius taken to be constant; p is the pressure; g gravitational acceleration; ρ_I the ice density; $\tau = \{\tau_{ij}\}$ is the stress tensor, and it is important to note that the divergence $\nabla \cdot$ of a second order tensor in curvilinear coordinates contains some metric terms in addition to those appearing in the divergence of a vector (Appendix B). Unit vectors in the directions of the three coordinates are denoted $\hat{\mathbf{e}}_\phi$, $\hat{\mathbf{e}}_\theta$ and $\hat{\mathbf{e}}_z$. We use Glen's flow law [*Glen*, 1955] to relate the stress to the rate of strain $\dot{\epsilon}_{ij}$,

$$
\begin{aligned}
\tau_{ij} &= A(T)^{-\frac{1}{3}}\dot{\epsilon}^{\frac{1}{3}-1}\dot{\epsilon}_{ij} \\
\dot{\epsilon}^2 &= \dot{\epsilon}_{mn}\dot{\epsilon}_{mn}/2,
\end{aligned}
$$

where T is the ice temperature and $A(T)$ is the temperature dependence of ice viscosity, which we take to be that used by *Goodman and Pierrehumbert* [2003]. We assume the temperature varies linearly in depth from a prescribed surface temperature to the freezing temperature at the base of the ice, which we assume constant. We use two different prescribed surface temperature latitudinal profiles which we refer to as the "warm" and "cold" profiles. These surface temperatures are a smooth fit to those calculated by the NCAR Community Atmospheric Model assuming a surface albedo of 0.6 at high (10^5 ppm) and low (100 ppm) CO_2 values (D. Abbot et al, SNOWMIP2: Deep Snowball and Snowball deglaciation model intercomparison, manuscript in preparation, 2012). The boundary conditions are that the dot product of stress with the normal vector vanishes at the top of the ice, and is equal to the hydrostatic pressure force normal to the bottom of the ice [*MacAyeal*, 1997],

$$
\begin{aligned}
(\tau - p\mathbf{I}) \cdot \hat{\mathbf{n}}_s &= 0, \\
(\tau - p\mathbf{I}) \cdot \hat{\mathbf{n}}_b &= -\hat{\mathbf{n}}_b p_w,
\end{aligned}
\tag{2}
$$

where $\hat{\mathbf{n}}_s$ and $\hat{\mathbf{n}}_b$ are normal vectors to the ice surface and bottom, and $\mathbf{I}$ is the unit tensor (matrix). Because the component of the stress parallel to the ice surface vanishes at the top and bottom (friction with the ocean and atmosphere is negligible), a very good approximation is to assume that the horizontal ice velocities are independent of depth [e.g., *Weertman*, 1957; *MacAyeal and Barcilon*, 1988]. Additionally, the vertical scale of the floating ice is much smaller than Earth's radius r, and we therefore employ the "thin shell" approximation, in which r is assumed to be constant. The very large aspect ratio (thousands of km in the horizontal dimension, vs hundreds of meters in the vertical) implies that the vertical velocities may be assumed to be very small relative to the horizontal ones. These assumptions lead to the following approximation for the symmetric rate of strain tensor in spherical coordinates (Appendix A),

$$\dot{\epsilon} \approx \begin{pmatrix} \frac{1}{r\sin\theta}\left(\partial_\phi u + v\cos\theta\right) & \cdot & \cdot \\ \frac{1}{2r}\left(\frac{1}{\sin\theta}\partial_\phi v + \sin\theta\,\partial_\theta(u/\sin\theta)\right) & \frac{1}{r}\partial_\theta v & \cdot \\ 0 & 0 & \partial_z w \end{pmatrix}, \quad (3)$$

where entries marked by dots above the diagonal are equal to their symmetric counterparts below the diagonal. Note in particular that $\dot{\epsilon}_{\theta z} = \dot{\epsilon}_{\phi z} \approx 0$ so that $\tau_{\theta z} \approx 0$, $\tau_{\phi z} \approx 0$ as well.

[12] Following *Morland* [1987] and *MacAyeal* [1997], we integrate the above momentum equations from top to bottom and use the boundary conditions (2) to find the final set of ice shelf equations in spherical coordinates (Appendix A2),

$$0 = \frac{1}{\sin\theta}\partial_\phi\left[B\left(2\frac{1}{\sin\theta}\left(\partial_\phi u + v\cos\theta\right) + \partial_\theta v\right)\right]$$
$$+ \frac{1}{\sin\theta}\partial_\theta\left[B\frac{1}{2}\left(\partial_\phi v + \sin^2\theta\partial_\theta(u/\sin\theta)\right)\right]$$
$$+ \cot\theta\, B\frac{1}{2}\left(\frac{1}{\sin\theta}\partial_\phi v + \sin\theta\,\partial_\theta(u/\sin\theta)\right)$$
$$- \frac{1}{\sin\theta}g\rho_I(1-\mu)hh_\phi \quad (4)$$

$$0 = \frac{1}{\sin\theta}\partial_\phi\left[B\frac{1}{2}\left(\frac{1}{\sin\theta}\partial_\phi v + \sin\theta\,\partial_\theta(u/\sin\theta)\right)\right]$$
$$+ \left[\frac{1}{\sin\theta}\partial_\theta(B\sin\theta\partial_\theta v) + \partial_\theta\left(B\frac{1}{\sin\theta}\partial_\theta(v\sin\theta)\right)\right]$$
$$+ \partial_\theta\left(B\frac{1}{\sin\theta}\partial_\phi u\right) - \cot\theta\, B\frac{1}{\sin\theta}\left(\partial_\phi u + v\cos\theta\right)$$
$$- g\rho_I(1-\mu)hh_\theta \quad (5)$$

$$B = \frac{1}{r}h\left\langle A(T)^{-\frac{1}{3}}\right\rangle\dot{\epsilon}^{\frac{1}{3}-1} \quad (6)$$

$$\dot{\epsilon}^2 = \frac{1}{2}\left(\dot{\epsilon}_{\phi\phi}^2 + \dot{\epsilon}_{\theta\theta}^2 + (\dot{\epsilon}_{\phi\phi} + \dot{\epsilon}_{\theta\theta})^2 + 2\dot{\epsilon}_{\phi\theta}^2\right) \quad (7)$$

$$h_t + \frac{1}{r\sin\theta}\partial_\phi(uh) + \frac{1}{r\sin\theta}\partial_\theta(\sin\theta\, vh) = \kappa\nabla^2 h + S(\phi,\theta), \quad (8)$$

where $\mu = \rho_I/\rho_w$, and $\langle\rangle$ denotes an average over the vertical dimension, where the temperature varies linearly in depth as

explained above [*Goodman and Pierrehumbert*, 2003]. An improved and more consistent treatment of the vertical averaging procedure is described by *Campbell et al.* [2011]. The above thickness equation is a statement of mass conservation, and the diffusion term is included for numerical reasons to make sure the solution is smooth. While we use the diffusion term merely as a numerical aid, it may also crudely represent snowdrift at the surface, which would tend to smooth thickness variations (although snow fall rate should be extremely small in a Snowball scenario). We keep the diffusion coefficient as small as allowed by the numerics, and the diffusion term is accordingly negligible relative to thickness advection throughout the domain. The forcing $S(\phi, \theta)$ represents the accumulated effect of surface and internal melting and sublimation, as well as basal freezing and melting of ice.

[13] The boundary conditions for the above equations are no normal flow into the north and south boundaries, and periodic boundary conditions in the east-west direction. In addition we prescribe no normal-flow and no slip conditions for the velocity field at continental boundaries, which is equivalent to assuming coastal boundaries are vertical. Zero normal derivatives of the thickness are prescribed for the advection-diffusion thickness equation at the north and south boundaries as well as at continental boundaries.

[14] It is useful to write explicitly the equations for the axisymmetric one-dimensional model which ignores continents, in which case there is no dependence on ϕ and the zonal velocity u is assumed to vanish,

$$0 = \left[\frac{1}{\sin\theta}\partial_\theta(B\sin\theta\partial_\theta v) + \partial_\theta\left(B\frac{1}{\sin\theta}\partial_\theta(v\sin\theta)\right) - \cot^2\theta\, Bv\right]$$
$$- g\rho_I(1-\mu)hh_\theta \quad (9)$$

$$B = \frac{1}{r}h\left\langle A(T)^{-\frac{1}{3}}\right\rangle\dot{\epsilon}^{\frac{1}{3}-1} \quad (10)$$

$$\dot{\epsilon}^2 = \left(\dot{\epsilon}_{\phi\phi}^2 + \dot{\epsilon}_{\theta\theta}^2 + \dot{\epsilon}_{zz}^2\right)/2 \quad (11)$$

$$\dot{\epsilon}_{zz} = -(\dot{\epsilon}_{\phi\phi} + \dot{\epsilon}_{\theta\theta}) \quad (12)$$

$$h_t + \frac{1}{r\sin\theta}\partial_\theta(\sin\theta\, vh) = \kappa\nabla^2 h + S(\theta). \quad (13)$$

[15] This one-dimensional model is different from that used in previous studies [e.g., *Goodman and Pierrehumbert*, 2003; *Goodman*, 2006; *Pollard and Kasting*, 2005, 2006]. First, it more accurately accounts for the lateral geometry following the *Morland* [1987] and *MacAyeal* [1997] formulation, which leads to the second term in the above momentum equation. Second, it includes the spherical coordinate correction to the divergence of the stress tensor (third term in the momentum equation). The spherical coordinate correction term arises mathematically from the additional set of geometric correction terms in the expression of the divergence of a second order tensor relative to that of a vector (Appendix B). Physically this term is due to the stress element $\tau_{\phi\phi}$ appearing in the θ (meridional) direction momentum balance (see term including $\tau_{\phi\phi}$ in

Table 1. List of Model Experiments[a]

Experiment	Model	T_{surf}	Land	Figure
3	1-D	warm	-	1
4	1-D	cold	-	1
5	2-D	warm	-	-
7	2-D	warm	630Myr	-
8	2-D	cold	630Myr	-
9	2-D X2	warm	630Myr	2
10	2-D X2	cold	630Myr	2

[a]X2 means resolution of 176 grid points, otherwise 89 points are used. "Warm" refers to the prescribed surface temperature seen in Figure 1c, while "cold" refers to that shown in Figure 1d.

equation (A10)). This stress element represents the unit force in the ϕ direction, acting on a unit surface perpendicular to this same direction. It is non zero even in the axisymmetric case because $\dot{\epsilon}_{\phi\phi}$ does not vanish in this case as explained below. To see why a stress element representing a force in the ϕ direction appears in the momentum equation for the θ direction, consider a small volume element in spherical coordinates, $(d\phi, d\theta, dr)$. Note that the faces of this element that are perpendicular to the ϕ direction have a slightly different northward slope at longitudes ϕ and at $\phi + d\phi$. As a result, the net force in the ϕ direction due to the sum of $\tau_{\phi\phi}$ acting on these faces has a component in the θ direction, leading to the above term. Finally, this equation includes the contribution of the non-vanishing $\dot{\epsilon}_{\phi\phi}$ element in the effective viscosity, again due to the spherical coordinates used as explained after equation (3). *Goodman and Pierrehumbert* [2003], as well as *Li and Pierrehumbert* [2011] noted the existence of this effect, but argued that it was inconsequential in comparison with the much larger effect of temperature on ice rheology, and the much larger uncertainty in ice rheology coefficients. Unlike in Cartesian coordinates, $\dot{\epsilon}_{\phi\phi}$ does not vanish in the axisymmetric case where there is no dependence on ϕ and where $u = 0$. It is equal then to $v \cot \theta / r$, representing the fact that a fluid line element oriented in the east-west direction and advected by a uniform northward flow will shrink due to the convergence of the longitude lines. This modifies the effective viscosity as seen in equations (10) and (11).

[16] This fuller treatment of spherical coordinates precludes the explicit integration of the velocity equation and the derivation of a single equation for the thickness, as was possible using the simpler equations of previous studies. Nevertheless the fuller equations (9)–(13) are easily solved numerically using a combination of a tri-diagonal solver for the momentum equation (iterated to account for the nonlinear effective viscosity [*MacAyeal*, 1997]), and time stepping of the thickness equation.

[17] Eliminating the spherical corrections and the more accurate treatment of the bottom and surface slopes and boundary conditions (equivalent to making a small-slope approximation at these boundaries), our 1-D equation reduces to a simpler one, in which only the first term is left in the square brackets in the momentum equation (9), in addition to the pressure gradient term. Neglecting also the contribution of $\dot{\epsilon}_{\phi\phi}$ to the rate of strain, we get a simpler equation which may be integrated once in co-latitude to lead to the *Goodman and Pierrehumbert* [2003] equation. The constant of integration from this first integration then plays a parallel role to that of

the "body force" introduced by those authors to represent the pressure force due to the collision of ice from the north and south hemispheres, and to allow the velocity to vanish in the case of symmetric forcing with respect to the equator. Instead of postulating this force, we can use the constants of integration to satisfy the boundary conditions of vanishing velocity at the north and south ends of the domain, and when the forcing $S(\theta)$ is symmetric in latitude, the equatorial velocity vanishes as expected. Using a constant of integration instead of a prescribed body force is also discussed in the supplementary material of *Li and Pierrehumbert* [2011].

[18] We solve the 2-D and 1-D model equations numerically using finite difference approximation over a near-global domain from 80°S to 80°N, prescribing no-normal flow into the northern and southern boundaries. We use a resolution of 176 × 176 grid points in the 2-D cases shown in the figures below, and of 89 grid points in the 1-D case. The finite difference formulation is based on an A-grid (all variables defined at the same point) and center differencing. In the grid points adjacent to landmasses, we estimate the pressure gradient terms and the effective viscosity using the one-sided finite difference approximation. The momentum equations are solved following standard procedure by iterating on the effective viscosity [*MacAyeal*, 1997].

[19] The prescribed time-independent, latitude-dependent, net melting/freezing/sublimation are from the *Pollard and Kasting* [2005, Figure 4c] model for the case of bubbly ice (dashed lines, smoothed before used here). We do not differentiate between surface and basal melting/freezing, and therefore do not include feedbacks between basal melting/freezing and ice thickness via the balance between heat diffusion within the ice cover and geothermal heat flux [*Goodman and Pierrehumbert*, 2003]. The global integral of the specified source function vanishes, and the flow and source function can therefore only redistribute thickness across the domain. As expected in the absence of the thickness-dependent basal melting, the domain-averaged thickness is set by the initial conditions, and is therefore not uniquely determined by the model parameters. We initialize integrations with an average thickness of 1000 meters.

[20] Because our forcing corresponds to the bubbly (reflecting) ice case of *Pollard and Kasting* [2005], the thickness variations we calculate may be underestimating those that could be calculated by including additional effects involving the optical properties of the ice etc. Ignoring other feedbacks, such as dependence of basal melting/freezing on ice thickness may also significantly affect our solution. Addressing these additional effects well would require a full ocean general circulation model that would calculate the ocean heat transports and temperature field and, from that, the basal melting and freezing. This is left for a future study.

[21] The model code is written in Matlab and is available at www.seas.harvard.edu/climate/eli/Downloads.

3. Numerical Results

[22] Table 1 lists the different model experiments we have performed. All shown results represent the steady state model solution, obtained by running the model for at least one hundred thousand years. The results of the 1-D model, which ignores land masses, are shown in Figure 1. Consistent with previous studies and with the scaling arguments given in
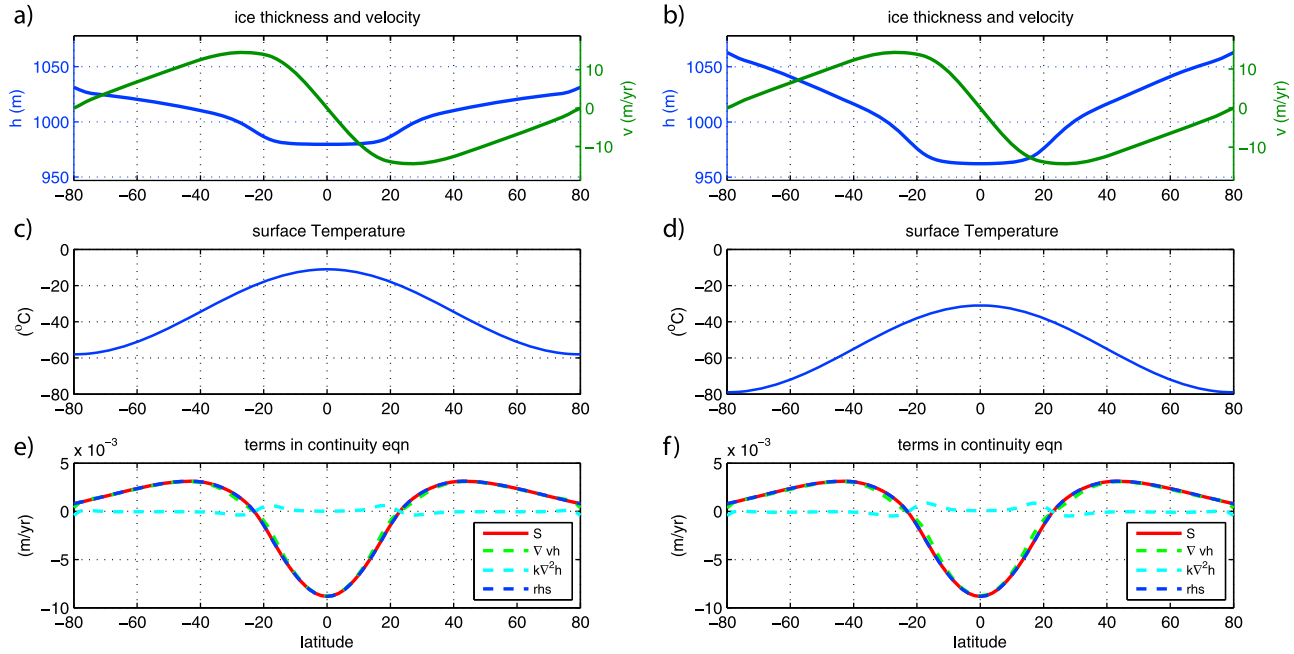
Figure 1. Steady state results of the 1-D model (equations (9)–(13)). (a, c, e) "Warm" (experiment 3 in Table 1) and (b, d, f) "cold" case (experiment 4). (Figures 1a and 1b) Ice thickness and meridional velocity as function of latitude. (Figures 1c and 1d) Specified surface temperature. (Figures 1e and 1f) Terms in the continuity equation (13) ("rhs" in the legend denotes the sum of the advection and diffusion terms, which should exactly balance the source S in a steady state).

section 4.2, this model predicts a very small thickness difference between the pole and the equator when optical/dust effect are not included (comparable to the (*Pollard and Kasting* [2005, Figure 4f], dash line representing bubbly ice); note the discussion in *Li and Pierrehumbert* [2011] regarding the larger difference found in *Goodman and Pierrehumbert* [2003]). The model results show an ice thickness difference of about 100 meters between the equator and pole for the cold case, and only 40 meters for the warm case. The warmer temperatures make the ice softer, as expected, and therefore lead to even smaller thickness gradients. The small meridional ice thickness gradient in both cases demonstrates the effectiveness of the ice flow in effectively homogenizing ice thickness, as pointed out by *Goodman and Pierrehumbert* [2003]. Such a uniformly thick ice does not allow light penetration into the ocean, with implications to photosynthesis as discussed in the introduction. Our two-dimensional model produces identical results to the 1-D model when no continent is included (experiment 5, Table 1, not shown).

[23] The results of the two-dimensional model for a continental configuration roughly following a Neoproterozoic reconstruction for 630 Myr [*Li et al.*, 2008] are shown in Figure 2. The land configuration was modified to eliminate features such as single grid point openings in topography that may lead to numerical problems. The figure shows the flow, thickness and $\log_{10}$ of the effective viscosity,

$$\nu_{\text{eff}} = \left\langle A(T)^{-\frac{1}{3}} \right\rangle \dot{\epsilon}^{\frac{1}{3}-1} \qquad (14)$$

for both a "warm" surface temperature corresponding to the high-CO_2 near-melting case and for the cold, low-CO_2 case.

[24] The thickness variations are clearly much larger than in the axisymmetric case. Because the constricted ocean area is small, the zonally averaged thickness and velocity fields may not be very different from those of the one dimensional model, but the local thickness differences are clearly much larger. This is especially evident in constricted areas such as between the main landmass and the two small continents to the east and west of it, and in particular between the global ocean and the marginal (constricted) sea in the middle of the major landmass. In this latter case the ice flow through the narrow passages needs to balance to total ice melting and evaporation within the constricted sea. Therefore the larger the area of the sea and the narrower are the straits, the faster is the ice flow expected to be. These results are consistent with the general message of *Campbell et al.* [2011] [see also *Warren et al.* 2002] that when the flow is limited by the continental geometry, significant ice thickness differences develop. We note that in addition to these constricted ocean locations, Figure 2 also shows significant thickness variations south of the main continent, especially in the "cold" case (Figure 2b). The thickness variations in this specific location are likely affected by the artificial boundary at 80N placed there in order to avoid the coordinate singularity at the pole, yet these results demonstrate that thickness variations due to the interaction of geometry and flow occur in a wider range of situations than was possible to discuss in previous studies.

[25] The thickness variations are again larger for the colder temperature case, when the ice is stiffer and requires larger pressure (thickness) gradients to drive the flow needed to balance net sublimation/melting within the constricted sea. The next section provides a scaling expression for this effect as well as for the global axisymmetric case. Note that
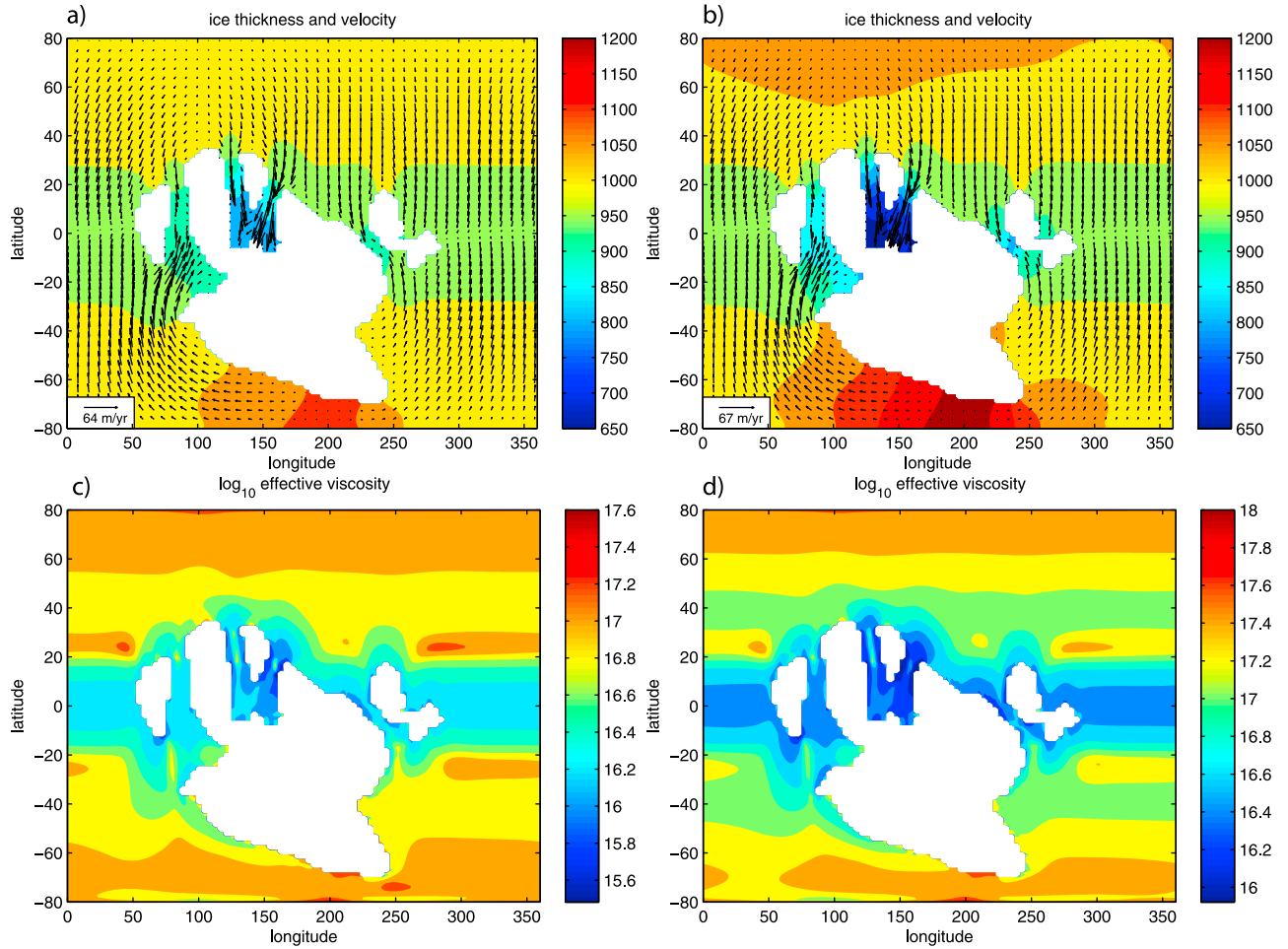
Figure 2. (a, b) Steady state results of the 2-D nonlinear model for ice thickness (in meters, shown by color contours), and ice velocity field (arrows, m/year, only every fourth velocity vector is drawn). Results are shown for a continental configuration motivated by a 630 Myr reconstruction, based on experiments 9 (warm, Figures 2a and 2c) and 10 (cold, Figures 2b and 2d), see Table 1. (c, d) The $\log_{10}$ of the corresponding effective viscosity given by equation (14). Axes indicate degrees longitude and latitude.

the velocity field is not very different between the warm and cold runs (see maximum velocities indicated in Figure 2) and this may be understood as follows. The specified source/ sink function $S(\phi, \theta)$ needs to be balanced by ice transport convergence, $\nabla \cdot (\mathbf{u}h)$. Given that the source function is constant in our runs, and if the thickness fields are not very different to zeroth order, this implies that the velocity field is, to a good approximation, set by the source function. Changes in the ice thickness between different runs would lead to changes in the velocity set by the source function. In turn, the thickness gradients that are required to drive this velocity field do depend on the ice viscosity and therefore on the temperature, as can be seen in Figures 1 and 2. It is possible to use our model results to identify and analyze the weak dependence of the flow field on the temperature, because the model does not include many other processes that could mask this result. This is an advantage of neglecting effects such as the dependence of the basal melting and freezing on the ice thickness and the effects of non-bubbly ice on the absorption of radiation.

[26] The temperature field implied by our model formulation is a three dimensional combination of the prescribed meridional surface temperature profile shown in Figures 1c and 1d, and the assumed linear vertical temperature profile from the prescribed surface temperature to the (assumed constant) melting temperature at the base of the ice. The ice flow field advects this temperature field and should lead, in principle, to a complex 3-D temperature distribution. This advection effect is neglected here, as well as strain heating generated within the ice, and horizontal diffusion. We can estimate how important the advection might be in different areas of the ice flow. Neglecting this advection is a sensible approximation only if the timescale of changes to the temperature due to vertical diffusion, which sets the linear vertical temperature profile, is shorter than that due to meridional advection. We therefore plot the following non-dimensional ratio, effectively a Peclet number, in Figure 3,

$$Pe = \frac{v(r\sin\theta)^{-1}\partial(\sin\theta T)/\partial\theta}{\kappa_i \partial^2 T/\partial z^2} \approx \frac{v(r\sin\theta)^{-1}\partial(\sin\theta T)/\partial\theta}{\kappa_i(T_{surface} - T_{freezing})/h^2} \quad (15)$$
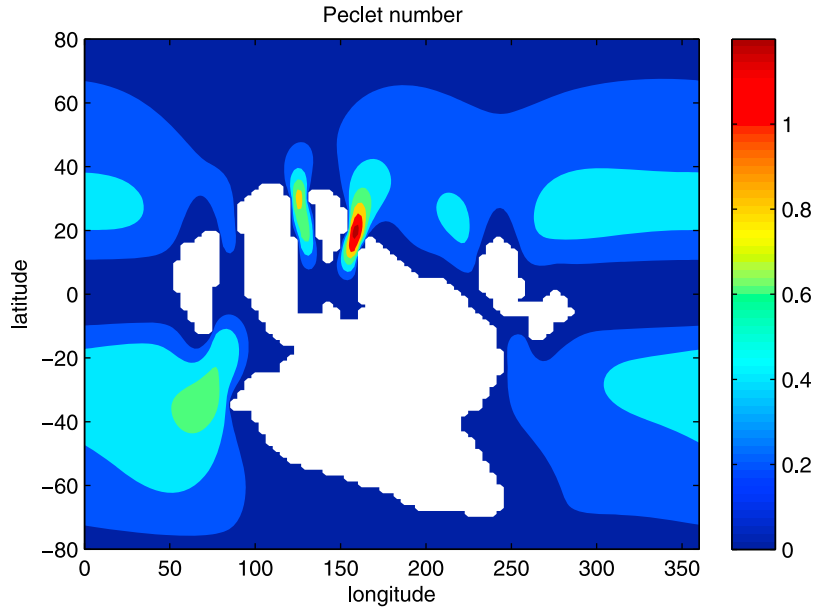
Peclet number

Figure 3. A nondimensional Peclet-like ratio of the temperature time rate of change due to horizontal advection vs due to vertical diffusion (equation (15)). Axes indicate degrees longitude and latitude.

where κ_i is the molecular heat diffusivity in ice, different from the (mostly numerical) horizontal diffusivity term appearing above in the mass conservation/thickness equation. Figure 3 shows that while temperature advection may be neglected in most areas (where the ratio is significantly smaller than one), it is not negligible in some key areas, in particular in narrow straights characterized by more rapid flow, where the ratio may be closer to, or even larger than, one. While these areas are quite isolated, it is clear that neglecting the effects of advection on the ice temperature is not justified there.

[27] Comparing the 2-D results based on a 176×176 grid to a solution on an 89×89 grid (experiments 7, 8 vs 9, 10, Table 1, figures not shown) shows that differences are not large. Ice thickness within the constricted sea is about 50 meters thinner in the coarser runs, indicating that numerical convergence of the solution as function of the model resolution has not been completely reached (as is often the case in global climate models). This is most likely due to insufficient resolution within the channels leading to the constricted sea. This problem, which often occurs in ocean models that cannot resolve critical narrow straights and sills (e.g., Straits of Gibraltar), may be resolved in future studies by either local grid refinement or by a parameterization of the channel flow, replacing the attempt to explicitly resolve the flow there. These solutions are beyond the scope of the present study.

4. Scaling Estimate of Ice Thickness Variations

[28] In this section we consider scaling estimate for thickness variations in two cases: a constricted sea fed by a long narrow channel, and a global, axisymmetric ocean.

4.1. Constricted Sea

[29] Consider a sea of area $\mathcal{A}$, linked to the ocean via a channel of length L and width W such that $L \gg W$. The ice thickness inside the sea, h_s, may be assumed uniform as a result of efficient ice flow equilibration, and we denote the open ocean ice thickness outside of the channel h_o. Denoting the ice velocity in the channel as V and the average sublimation/melt rate within the sea as b, the mass balance scaling for the ice cover of the sea is given by,

$$V h_o W \sim \mathcal{A} b. \tag{16}$$

[30] Another relation may be obtained from the ice shelf momentum balance equations [*Morland*, 1987; *MacAyeal*, 1997]. Let y be the along-channel coordinate and assume that $u = 0$; let also n be the Glen's flow law constant taken in our model equations above to be 3. The ice shelf along-channel (v) momentum equation,

$$0 = \partial_x \left(B \frac{1}{2}(u_y + v_x) \right) + \partial_y \left(B(u_x + 2v_y) \right) - g\rho_I(1-\mu)hh_y$$

$$B \equiv h \left\langle A(T)^{-\frac{1}{n}} \right\rangle \dot{\epsilon}^{\frac{1}{n}-1}$$

$$\dot{\epsilon}^2 \approx \frac{1}{2} \left(u_x^2 + v_y^2 + (u_x + v_y)^2 + \frac{1}{2}(u_y + v_x)^2 \right),$$

reduces to

$$0 = \partial_x(B\frac{1}{2}v_x) + \partial_y(B2v_y) - g\rho_I(1-\mu)hh_y$$

$$B \equiv h \left\langle A(T)^{-\frac{1}{n}} \right\rangle \dot{\epsilon}^{\frac{1}{n}-1}$$

$$\dot{\epsilon}^2 \approx \frac{1}{2} \left(2v_y^2 + \frac{1}{2}v_x^2 \right) \approx \frac{1}{4}v_x^2,$$

where the assumed large channel aspect ratio, $L/W \gg 1$ leads to $\dot{\epsilon} \approx v_x/2$ on the last line above. The second term in the

y-momentum equation may be neglected if $L \gg W$ because it scales with L^{-2} while the first terms scales with W^{-2}. Assuming the velocity vanishes at the sides of the channel and is maximal at its center, we scale the cross-channel shear as $v_x \sim V/(W/2)$, so that the momentum equation scales as,

$$\frac{BV}{2(W/2)^2} \sim g\rho_I(1-\mu)h_o(h_o - h_s)/L. \qquad (17)$$

[31] Scaling the effective viscosity as

$$B \sim h_o \left\langle A(T)^{-\frac{1}{n}} \right\rangle \left(\frac{1}{2} \frac{V}{W/2} \right)^{\frac{1}{n}-1}, \qquad (18)$$

and substituting the velocity scale from the mass balance equation, we find an estimate for the thickness difference along the channel,

$$h_o - h_s \sim \frac{2L \left\langle A(T)^{-\frac{1}{n}} \right\rangle}{Wg\rho_I(1 - \rho_I/\rho_w)} \left(\frac{\mathcal{A}b}{h_0 W^2} \right)^{\frac{1}{n}}. \qquad (19)$$

This scaling is to be compared with the formula for an ice invasion length in rectangular-shaped (Red-Sea like) marginal sea used by *Campbell et al.* [2011] following *Nye* [1965]. The advantage of their formulation is that it is based on an exact formula rather than crude scaling as done here. The scaling here, though, accounts for the case where the constricted sea is not rectangular but has a wider area fed by a narrow channel, as motivated by the Neoproterozoic landmass reconstruction shown in Figure 2. It is clear from this scaling estimate that a constricted sea located in the low-latitudes where there is net ice sublimation and melting, will lead to higher thickness variations (thinner ice in the constricted sea) if the channel is longer (large L), narrower (small W), or if the sea itself has a larger area ($\mathcal{A}$), larger melt rate (b) or if the ice temperature is colder (via the dependence on $A(T)$, note that $A(T)$ increases with temperature, and therefore $\left\langle A(T)^{-\frac{1}{n}} \right\rangle$ gets smaller; that is, warmer temperatures lead to softer ice and to smaller thickness differences).

[32] Substituting order-of-magnitude values for the parameters based on the "warm" solution for constricted sea in the Neoproterozoic land configuration (Figure 2), $\mathcal{A} = (4000 \cdot 10^3)^2$ (m^2); $b = 6 \cdot 10^{-3}/(365 \cdot 24 \cdot 3600)$ (m/s); $L = 2500 \cdot 10^3$ (m); $W = 1000 \cdot 10^3$ (m); $h_o = 1000$ (m); $g = 9.8$ (m/s^2); $\rho_I = 900$ (kg/m^3); $\rho_w = 1024$ (kg/m^3); $T_f = 273.16$ (K); $T_s = T_f - 30$ (K); $n = 3$; where we chose the surface temperature to represent the location of the main channel leading to the constricted sea in the warm case shown in Figure 2a, we find $h_o - h_s \sim 108$ m. This estimate is of the same order, yet smaller than that calculated by the numerical solution (compare to the "warm" solution in Figures 2a and 2c). Note that our assumption of $L \gg W$ isn't strictly satisfied. We calculated the thickness difference along the channel assuming a single channel but the above land configuration actually has two such channels, so that the comparison is somewhat vague. It is possible that a marginal grid resolution in the passages leading to the constricted sea

biases the resolution, and the scaling itself cannot be expected to yield exact results, of course. But the scaling does make it clear that significantly larger thickness differences are to be expected in the case of a constricted marginal sea than when there are no marginal seas, e.g., because continents are ignored. Scaling for the case of no continents is presented in the following section.

4.2. Global Ocean, No Continents

[33] The 1-D momentum and steady mass conservation equations (9) and (13) scale, correspondingly, as

$$2\frac{1}{r}h \left\langle A(T)^{-\frac{1}{3}} \right\rangle \left(\frac{v}{r} \right)^{\frac{1}{n}} \sim g\rho_I(1 - \rho_I/\rho_w)h\Delta h/r$$

$$vh/r \sim \Delta S$$

where the factor two on the left hand side of the momentum equation accounts for the first two terms in (9) and $\Delta S = S_{\max} - S_{\min}$. Together, these lead to a scaling for the thickness difference between the equator and the pole, Δh,

$$\Delta h \sim \frac{2 \left\langle A(T)^{-\frac{1}{3}} \right\rangle (\Delta S/[h])^{\frac{1}{n}}}{g\rho_I(1 - \rho_I/\rho_w)}. \qquad (20)$$

Substituting order of magnitude scales, $\Delta S = 12 \cdot 10^{-3}$/yr (m/s); $[h] = 1000$ (m); $g = 9.8$ (m/s^2); $\rho_I = 900$ (kg/m^3); $\rho_w = 1024$ (kg/m^3); $T_f = 273.16$ (K); $T_s = T_f - 30$ (K); $n = 3$ we find $\Delta h \sim 34$ m. This estimate is quite close to the numerical solution of the "warm" 1-D case in Figure 1. Rather than specifying the thickness scale as we did above, one could calculate it by balancing the diffusive heat flux through the ice with the geothermal heat flux F_{geo}, such that $[h] = \kappa\Delta T/F_{geo}$. Overall, the scaling estimates of this and the previous sections predict a much weaker thickness difference if continents are neglected, consistent with the numerical solutions.

5. Conclusions

[34] Ice flow over a Snowball ocean was shown to be an important factor participating in the determination of ice thickness over the ocean [*Goodman and Pierrehumbert*, 2003], and has received significant attention in recent years [*Warren et al.*, 2002; *Pollard and Kasting*, 2005; *Goodman*, 2006; *Warren and Brandt*, 2006; *Pollard and Kasting*, 2006; *Campbell et al.*, 2011; *Li and Pierrehumbert*, 2011]. These studies all use local models or one-dimensional global (latitude-only) models, formulated in a way that was difficult to extend to two dimensions (both longitude and latitude). This paper attempts to make progress on two different fronts related to this ice flow problem. First, we study the effects of continental constriction on ice flow and ice thickness in an ice-covered ocean in a Snowball-Earth scenario using a global model with reconstructed Neoproterozoic landmass configuration. Second, we provide a formulation of the ice flow problem in two dimensions on a sphere that should allow coupling such ice flow models to ocean and atmospheric general circulation models. This formulation is a

very simple extension of the well known ice shelf equations from glaciology [e.g., *Morland*, 1987; *MacAyeal*, 1997] to spherical coordinates.

[35] *Campbell et al.* [2011] used a formula derived by *Nye* [1965] to show that the invasion by ice into an idealized rectangular-shaped marginal sea (Red-Sea like) is limited by friction with the sidewalls and that this may lead to significant ice thickness variations within such a sea in regions of net sublimation. Our numerical simulations show that, consistent with the original idea of *Campbell et al.* [2011], continental constriction indeed leads to ice thickness variations in additional cases. This includes relatively narrow areas between sub-continents, and marginal seas whose entrance is constricted by landmass geometry. In addition to numerical solutions, we present scaling estimates of the thickness variations in both the case of a global ocean with no continents and in the case of a marginal sea fed by a relatively narrow channel. The scaling estimates are compared to the numerical solutions and are found to somewhat underestimate them, but are of the right order of magnitude.

[36] We formulated the ice flow problem starting with the equations of motion (Stokes equation) rather than from the *Weertman* [1957] estimate for the deformation rate of ice shelves. This allowed us to extend the formulation to two dimensions, which is not possible starting from the Weertman deformation rate formula. In addition, we show that in a model that depends on latitude only, a careful formulation of the lateral geometry and boundary conditions following *Morland* [1987], *MacAyeal and Barcilon* [1988], and *MacAyeal* [1989, 1997], as well as the effects of spherical coordinates, leads to additional terms in the model equations which were not included in previous studies. In particular, our formulation involves two integrations of the momentum equations in order to solve for the ice velocity. The constants of integration play a role parallel to that of the body force introduced by *Goodman and Pierrehumbert* [2003], allowing the meridional ice velocity to vanish at the equator in a model that's symmetric about the equator. We emphasize that the main qualitative result of the works which pioneered the study of ice flow in a Snowball ocean is still valid: ice flow effectively homogenizes ice thickness across the global ocean where the flow is not constricted by continents.

[37] While we were able to make significant progress in several ways, many related and important issues remain open. Our model ignores the flow of land ice toward the constricted sea. We anticipate that an attempt to simulate ice flow in a global ocean into marginal seas whose opening is small will run into numerical resolution limits. Rather than increasing the global resolution, one would need to resort to either local grid refinement, or to a parameterization of the ice flow in narrow straights, as is routinely done in coarse resolution ocean models that cannot resolve critical narrow straights and sills (e.g., Straits of Gibraltar). The poles pose a problem to the numerics in standard spherical coordinates as they do in oceanic and atmospheric models, and one could resort to alternative grids where the poles are moved to over a landmass [e.g., *Voigt et al.* 2011], or where Earth's surface is mapped into a cube as is done in current state-of-the-art ocean models [*Adcroft et al.*, 2004].

[38] Having concentrated on ice flow alone, we ignored all thermodynamic, dust and optical effects that are known to be important processes in setting ice thickness in a Snowball scenario [*Warren et al.*, 2002; *Goodman and Pierrehumbert*, 2003; *McKay*, 2000; *Pollard and Kasting*, 2005, 2006; *Warren and Brandt*, 2006; *Goodman*, 2006; *Abbot and Pierrehumbert*, 2010; *Li and Pierrehumbert*, 2011; *Pierrehumbert et al.*, 2011]. Instead, we prescribed the net source/sink of ice due to accumulation, freezing, melting and sublimation as time independent forcing fields based on the values calculated by *Pollard and Kasting* [2005]. While this allowed us to isolate the effects of ice flow, the ignored additional factors can make the thickness variations significantly larger, possibly leading to thin ice cover over constricted seas and low-latitudes, with implications for survival of life discussed by *Campbell et al.* [2011]. We cannot discuss such implications given that we neglected these important factors.

[39] It should be noted that the glaciological literature has dealt extensively with ice shelves, their dynamics, collapse, existence of rifting and fracturing during the flow through channels [e.g., *Doake et al.*, 1998; *Doake and Vaughan*, 1991; *MacAyeal et al.*, 2003; *Rott et al.*, 1996; *Vieli et al.*, 2006; *Weis et al.*, 1999; *van der Veen*, 1999]. The resulting lessons are of obvious relevance to the dynamics of ice flow over a Snowball ocean, as well as to the existence of refuges within ice shelf cracks.

[40] Given these many idealizations, we emphasize that this study is meant to be a process study focusing on one specific dynamical factor, not a realistic simulation of Neoproterozoic ice thickness. We also assume ice thickness to be large everywhere, and the formulation here would need to be extended if thin ice cover or ice-free ocean develops, or for a study of transient Snowball initiation and an invasion of the ocean by thick ice.

[41] In spite of its obvious limitations, this study is a first step toward coupling Snowball ice flow models to general circulation ocean and atmospheric models. This, in turn, will allow an improved representation of the basal and surface melting, freezing sublimation and snow accumulation and should help making these models more accurate.

Appendix A: Derivation of Model Equations

A1. Surface and Bottom Boundary Conditions

[42] The upper and lower boundary momentum conditions may be written [*MacAyeal*, 1997],

$$\begin{aligned} \boldsymbol{\sigma} \cdot \hat{\mathbf{n}}_s &= 0, \\ \boldsymbol{\sigma} \cdot \hat{\mathbf{n}}_b &= -\hat{\mathbf{n}}_b p_w, \end{aligned} \quad (A1)$$

where $\mathbf{n}_s$ and $\mathbf{n}_b$ are the outward-pointing normal vectors at the surface and the bottom, respectively. The stress tensor element σ_{ij} is the force in the i direction acting on a face perpendicular to the j direction, so that $\sigma_{ij}n_j$ is the total force in the i direction on a unit area along the ice surface. This force vanishes at the surface and is equal to the hydrostatic water pressure p_w at the bottom of the ice. Defining the deviatoric stress as $\tau_{ij} = \sigma_{ij} - \delta_{ij}\frac{1}{3}\sigma_{kk} = \sigma_{ij} + p\delta_{ij}$ (where δ_{ij} is the Kronecker delta, and the pressure is defined

as $p = -\frac{1}{3}\sigma_{kk}$), leads to the equivalent form of the boundary conditions

$$(\boldsymbol{\tau} - p\mathbf{I}) \cdot \hat{\mathbf{n}}_s = 0,$$
$$(\boldsymbol{\tau} - p\mathbf{I}) \cdot \hat{\mathbf{n}}_b = -\hat{\mathbf{n}}_b p_w. \tag{A2}$$

The normal vector to the surface elevation $s(\phi, \theta)$ is given by the gradient of $f(\phi, \theta, z) = z - s(\phi, \theta)$,

$$\hat{\mathbf{n}} = \frac{\nabla f}{\| \nabla f \|} = \frac{(-\frac{1}{r\sin\theta}s_\phi, -\frac{1}{r}s_\theta, 1)}{\| (-\frac{1}{r\sin\theta}s_\phi, -\frac{1}{r}s_\theta, 1) \|}. \tag{A3}$$

The boundary conditions (2) and (A2) in spherical coordinates then take the form,

$$(\tau_{\phi\phi} - p)\frac{1}{r\sin\theta}s_\phi + \tau_{\phi\theta}\frac{1}{r}s_\theta - \tau_{\phi z} = 0 \qquad z = s$$

$$\tau_{\theta\phi}\frac{1}{r\sin\theta}s_\phi + (\tau_{\theta\theta} - p)\frac{1}{r}s_\theta - \tau_{\theta z} = 0 \qquad z = s$$

$$\tau_{z\phi}\frac{1}{r\sin\theta}s_\phi + \tau_{z\theta}\frac{1}{r}s_\theta - (\tau_{zz} - p) = 0 \qquad z = s$$

$$(\tau_{\phi\phi} - p)\frac{1}{r\sin\theta}b_\phi + \tau_{\phi\theta}\frac{1}{r}b_\theta - \tau_{\phi z} = -\frac{1}{r\sin\theta}b_\phi g\rho_w\mu h \qquad z = b$$

$$\tau_{\theta\phi}\frac{1}{r\sin\theta}b_\phi + (\tau_{\theta\theta} - p)\frac{1}{r}b_\theta - \tau_{\theta z} = -\frac{1}{r}b_\theta g\rho_w\mu h \qquad z = b$$

$$\tau_{z\phi}\frac{1}{r\sin\theta}b_\phi + \tau_{z\theta}\frac{1}{r}b_\theta - (\tau_{zz} - p) = g\rho_w\mu h \qquad z = b \tag{A4}$$

where $\mu = \rho_I/\rho_w$ as above.

A2. Ice Shelf-Equations in Spherical Coordinates

[43] This derivation follows *Morland* [1987] and *MacAyeal* [1997], except for the use of spherical coordinates here (Alternatively, the same results can be derived by starting from the invariant formulation of *Schoof* [2006] and using expressions for the covariant derivatives in spherical coordinates). Let the coordinates (longitude, co-latitude, vertical) be denoted by (ϕ, θ, r) and the corresponding velocities be (u, v, w). Below, when we make the "thin shell" approximation, we switch to the coordinates (ϕ, θ, z) and treat r as a constant. The gradient, divergence of a vector and Laplacian are,

$$\nabla = \left(\frac{1}{r\sin\theta}\partial_\phi, \frac{1}{r}\partial_\theta, \partial_r\right)$$

$$\nabla \cdot \mathbf{v} = \frac{1}{r\sin\theta}\partial_\phi u + \frac{1}{r\sin\theta}\partial_\theta(\sin\theta v) + \frac{1}{r^2}\partial_r(r^2 w)$$
$$\approx \frac{1}{r\sin\theta}\partial_\phi u + \frac{1}{r\sin\theta}\partial_\theta(\sin\theta v) + \partial_z w$$

$$\Delta f = \frac{1}{r^2}\frac{\partial}{\partial r}\left(r^2\frac{\partial f}{\partial r}\right) + \frac{1}{r^2\sin\theta}\frac{\partial}{\partial\theta}\left(\sin\theta\frac{\partial f}{\partial\theta}\right) + \frac{1}{r^2\sin^2\theta}\frac{\partial^2 f}{\partial\phi^2}$$
$$\approx \partial_{zz}f + \frac{1}{r^2\sin\theta}\partial_\theta(\sin\theta\partial_\theta f) + \frac{1}{r^2\sin^2\theta}\partial_{\phi\phi}f, \tag{A5}$$

where we have made the approximation of a thin shell of ice whose thickness is much smaller than Earth's radius,

replacing r-derivatives with derivatives with respect to a local vertical coordinate z and treating r as a constant equal to Earth's radius. The (symmetric) rate of strain is (its elements above the diagonal are omitted),

$$\dot{\boldsymbol{\epsilon}} = \begin{pmatrix} \dot{\epsilon}_{\phi\phi} & \dot{\epsilon}_{\phi\theta} & \dot{\epsilon}_{\phi r} \\ \dot{\epsilon}_{\theta\phi} & \dot{\epsilon}_{\theta\theta} & \dot{\epsilon}_{\theta r} \\ \dot{\epsilon}_{r\phi} & \dot{\epsilon}_{r\theta} & \dot{\epsilon}_{rr} \end{pmatrix}$$

$$= \begin{pmatrix} \frac{1}{r\sin\theta}(\partial_\phi u + w\sin\theta + v\cos\theta) & \cdot & \cdot \\ \frac{1}{2r}\left(\frac{1}{\sin\theta}\partial_\phi v + \sin\theta\partial_\theta(u/\sin\theta)\right) & \frac{1}{r}(\partial_\theta v + w) & \cdot \\ \frac{1}{2}\left(\frac{1}{r\sin\theta}\partial_\phi w + r\partial_r(u/r)\right) & \frac{1}{2}\left(\frac{1}{r}\partial_\theta w + r\partial_r(v/r)\right) & \partial_r w \end{pmatrix}. \tag{A6}$$

[44] Simplifying the rate of strain tensor using the thin shell approximation (e.g., $\frac{1}{r^2}\partial_r(r^2 w) \approx \partial_z w$ and neglecting w_θ/r) as well as using the ice shelf approximation of neglecting $\dot{\epsilon}_{\theta z}, \dot{\epsilon}_{\phi z}$, and assuming the horizontal velocities are z-independent and much larger than the vertical velocity,

$$\dot{\boldsymbol{\epsilon}} \approx \begin{pmatrix} \frac{1}{r\sin\theta}(\partial_\phi u + v\cos\theta) & \cdot & \cdot \\ \frac{1}{2r}\left(\frac{1}{\sin\theta}\partial_\phi v + \sin\theta\partial_\theta(u/\sin\theta)\right) & \frac{1}{r}\partial_\theta v & \cdot \\ 0 & 0 & \partial_z w \end{pmatrix}. \tag{A7}$$

The momentum equations in vector form (1) are written explicitly in component form in spherical coordinates as,

$$0 = -\frac{1}{r\sin\theta}\partial_\phi p + \frac{1}{r\sin\theta}\partial_\phi\tau_{\phi\phi} + \frac{1}{r\sin\theta}\partial_\theta(\sin\theta\tau_{\theta\phi})$$
$$+ \frac{1}{r^2}\partial_r(r^2\tau_{r\phi}) + \frac{\tau_{r\phi}}{r} + \frac{\cot\theta}{r}\tau_{\theta\phi}$$

$$0 = -\frac{1}{r}\partial_\theta p + \frac{1}{r\sin\theta}\partial_\phi\tau_{\phi\theta} + \frac{1}{r\sin\theta}\partial_\theta(\sin\theta\tau_{\theta\theta}) + \frac{1}{r^2}\partial_r(r^2\tau_{r\theta})$$
$$+ \frac{\tau_{r\theta}}{r} - \frac{\cot\theta}{r}\tau_{\phi\phi}$$

$$0 = -\partial_r p - g\rho_I + \frac{1}{r\sin\theta}\partial_\phi(\tau_{r\phi}) + \frac{1}{r\sin\theta}\partial_\theta(\sin\theta\tau_{r\theta})$$
$$+ \frac{1}{r^2}\partial_r(r^2\tau_{rr}) - \frac{\tau_{\theta\theta} + \tau_{\phi\phi}}{r}, \tag{A8}$$

where the divergence of a second order tensor in curvilinear coordinates contains a set of metric corrections in addition to those appearing in the divergence of a vector (see an outline of the mathematical justification in Appendix B, and a heuristic discussion within the paper after equations (9)–(13)). These are the last two terms in the two horizontal momentum equation and the last term in the vertical momentum equation. Using the thin shell approximation and the ice shelf approximation $\tau_{\theta z} \approx 0$, $\tau_{\phi z} \approx 0$,

$$0 = -\frac{1}{r\sin\theta}\partial_\phi p + \frac{1}{r\sin\theta}\partial_\phi\tau_{\phi\phi} + \frac{1}{r\sin\theta}\partial_\theta(\sin\theta\tau_{\theta\phi}) + \frac{\cot\theta}{r}\tau_{\theta\phi} \tag{A9}$$

$$0 = -\frac{1}{r}\partial_\theta p + \frac{1}{r\sin\theta}\partial_\phi\tau_{\phi\theta} + \frac{1}{r\sin\theta}\partial_\theta(\sin\theta\tau_{\theta\theta}) - \frac{\cot\theta}{r}\tau_{\phi\phi}$$

(A10)

$$0 = -\partial_z p - g\rho_I + \partial_z\tau_{zz} - \frac{\tau_{\theta\theta} + \tau_{\phi\phi}}{r}.$$

(A11)

[45] Next, integrate the two horizontal momentum equations from top to bottom and use the Leibniz rule, and integrate the vertical equation first from top to z and then from top to bottom (all such integrals $\int_b^s$ are over depth, we drop the dz for brevity) to find,

$$0 = \frac{1}{r\sin\theta}\partial_\phi\int_b^s(\tau_{\phi\phi} - p) + \frac{1}{r\sin\theta}\partial_\theta\int_b^s(\sin\theta\tau_{\theta\phi})$$
$$- \frac{1}{r\sin\theta}s_\phi(\tau_{\phi\phi} - p)|_s + \frac{1}{r\sin\theta}b_\phi(\tau_{\phi\phi} - p)|_b - \frac{1}{r}s_\theta\tau_{\theta\phi}(s)$$
$$+ \frac{1}{r}b_\theta\tau_{\theta\phi}(b) + \frac{\cot\theta}{r}\int_b^s\tau_{\phi\phi}$$
$$0 = -\frac{1}{r}\partial_\theta\int_b^s p + \frac{1}{r\sin\theta}\partial_\phi\int_b^s\tau_{\phi\theta} + \frac{1}{r\sin\theta}\partial_\theta\int_b^s(\sin\theta\tau_{\theta\theta})$$
$$+ \frac{1}{r}s_\theta p(s) - \frac{1}{r}b_\theta p(b) - \frac{1}{r\sin\theta}s_\phi\tau_{\phi\theta}(s) + \frac{1}{r\sin\theta}b_\phi\tau_{\phi\theta}(b)$$
$$- \frac{1}{r}s_\theta\tau_{\theta\theta}(s) + \frac{1}{r}b_\theta\tau_{\theta\theta}(b) - \frac{\cot\theta}{r}\int_b^s\tau_{\phi\phi}$$
$$0 = \int_b^s\left(-(p(s) - p) - g\rho_I(s - z) + \tau_{zz}(s) - \tau_{zz}(z)\right)$$
$$- \frac{1}{r}\int_b^s\int_z^s(\tau_{\theta\theta} + \tau_{\phi\phi}).$$

(A12)

Using the top and bottom boundary conditions (A4) as well as that trace$(\tau_{ij}) = 0$,

$$0 = \frac{1}{r\sin\theta}\partial_\phi\int_b^s(\tau_{\phi\phi} - p) + \frac{1}{r\sin\theta}\partial_\theta\int_b^s(\sin\theta\tau_{\theta\phi})$$
$$- \frac{1}{r\sin\theta}b_\phi g\rho_w\mu h + \frac{\cot\theta}{r}\int_b^s\tau_{\theta\theta}$$
$$0 = -\frac{1}{r}\partial_\theta\int_b^s p + \frac{1}{r\sin\theta}\partial_\phi\int_b^s\tau_{\phi\theta} + \frac{1}{r\sin\theta}\partial_\theta\int_b^s(\sin\theta\tau_{\theta\theta})$$
$$- \frac{1}{r}b_\theta g\rho_w\mu h - \frac{\cot\theta}{r}\int_b^s\tau_{\phi\phi}$$
$$- \int_b^s p = -g\rho_I\frac{1}{2}h^2 + \int_b^s(\tau_{\phi\phi} + \tau_{\theta\theta}) - \frac{1}{r}\int_b^s\int_z^s(\tau_{\theta\theta} + \tau_{\phi\phi})$$

(A13)

Neglecting the $\mathcal{O}(h/r)$ terms in the third equation and substituting the remaining terms in the first two using $h = s - b$ and $s = (1 - \mu)h$,

$$0 = \frac{1}{r\sin\theta}\partial_\phi\int_b^s(2\tau_{\phi\phi} + \tau_{\theta\theta}) + \frac{1}{r\sin\theta}\partial_\theta\int_b^s(\sin\theta\tau_{\theta\phi})$$
$$+ \frac{\cot\theta}{r}\int_b^s\tau_{\theta\theta} - \frac{1}{r\sin\theta}g\rho_I(1 - \mu)hh_\phi$$
$$0 = \frac{1}{r\sin\theta}\partial_\phi\int_b^s\tau_{\phi\theta} + \frac{1}{r\sin\theta}\partial_\theta\int_b^s\sin\theta\tau_{\theta\theta} + \frac{1}{r}\partial_\theta\int_b^s(\tau_{\theta\theta} + \tau_{\phi\phi})$$
$$- \frac{\cot\theta}{r}\int_b^s\tau_{\phi\phi} - \frac{1}{r}g\rho_I(1 - \mu)hh_\theta.$$

(A14)

Using Glen's flow law to express the stress components in terms of the strain rates and therefore velocity components,

$$0 = \frac{1}{\sin\theta}\partial_\phi\left[B\left(2\frac{1}{\sin\theta}(\partial_\phi u + v\cos\theta) + \partial_\theta v\right)\right]$$
$$+ \frac{1}{\sin\theta}\partial_\theta\left[B\frac{1}{2}\left(\partial_\phi v + \sin^2\theta\partial_\theta(u/\sin\theta)\right)\right]$$
$$+ \cot\theta B\frac{1}{2}\left(\frac{1}{\sin\theta}\partial_\phi v + \sin\theta\partial_\theta(u/\sin\theta)\right)$$
$$- \frac{1}{\sin\theta}g\rho_I(1 - \mu)hh_\phi$$
$$0 = \frac{1}{\sin\theta}\partial_\phi\left[B\frac{1}{2}\left(\frac{1}{\sin\theta}\partial_\phi v + \sin\theta\partial_\theta(u/\sin\theta)\right)\right]$$
$$+ \left[\frac{1}{\sin\theta}\partial_\theta(B\sin\theta\partial_\theta v) + \partial_\theta\left(B\frac{1}{\sin\theta}\partial_\theta(v\sin\theta)\right)\right]$$
$$+ \partial_\theta\left(B\frac{1}{\sin\theta}\partial_\phi u\right) - \cot\theta\frac{1}{\sin\theta}B(\partial_\phi u + v\cos\theta)$$
$$- g\rho_I(1 - \mu)hh_\theta$$
$$B = \frac{1}{r}h\left\langle A(T)^{-\frac{1}{3}}\right\rangle\dot{\epsilon}^{\frac{1}{3}-1}$$
$$\dot{\epsilon}^2 = \frac{1}{2}\left(\dot{\epsilon}_{\phi\phi}^2 + \dot{\epsilon}_{\theta\theta}^2 + (\dot{\epsilon}_{\phi\phi} + \dot{\epsilon}_{\theta\theta})^2 + 2\dot{\epsilon}_{\phi\theta}^2\right)$$
$$h_t + \frac{1}{r\sin\theta}\partial_\phi(uh) + \frac{1}{r\sin\theta}\partial_\theta(\sin\theta vh) = \kappa\nabla^2 h + S(\phi, \theta),$$

(A15)

where $\langle\rangle$ denotes an average over the vertical dimension [see *Goodman and Pierrehumbert*, 2003]. These final equations appear in the text of the paper itself as equations (4)–(8).

Appendix B: Divergence of a Tensor

[46] Write the divergence operator as

$$\nabla\cdot = \hat{\mathbf{e}}_\phi\frac{1}{r\sin\theta}\partial_\phi + \hat{\mathbf{e}}_\theta\frac{1}{r}\partial_\theta + \hat{\mathbf{e}}_r\partial_r,$$

(B1)

and note that the unit vectors in spherical coordinates are not constants, such that, for example, $\partial_\theta\hat{\mathbf{e}}_\theta = -\hat{\mathbf{e}}_r$ [*Greenberg*, 1998].

[47] Applying the above divergence to a vector $\mathbf{v}$,

$$\nabla\cdot\mathbf{v} = (\hat{\mathbf{e}}_\phi\frac{1}{r\sin\theta}\partial_\phi + \hat{\mathbf{e}}_\theta\frac{1}{r}\partial_\theta + \hat{\mathbf{e}}_r\partial_r)\cdot(\hat{\mathbf{e}}_\phi u + \hat{\mathbf{e}}_\theta v + \hat{\mathbf{e}}_r w)$$

(B2)

we find that the derivatives of the unit vectors introduce a set of correction terms due to the non-Cartesian coordinates. To derive the divergence of a tensor (which yields a vector), write it as

$$\nabla\cdot\boldsymbol{\tau} = \left(\hat{\mathbf{e}}_\phi\frac{1}{r\sin\theta}\partial_\phi + \hat{\mathbf{e}}_\theta\frac{1}{r}\partial_\theta + \hat{\mathbf{e}}_r\partial_r\right)$$
$$\cdot(\hat{\mathbf{e}}_\phi\otimes\hat{\mathbf{e}}_\phi\tau_{\phi\phi} + \hat{\mathbf{e}}_\phi\otimes\hat{\mathbf{e}}_\theta\tau_{\phi\theta} + ...)$$

(B3)

where $\hat{\mathbf{e}}_\phi\otimes\hat{\mathbf{e}}_\theta$, for example, is a tensor whose only nonzero element is at the $(\phi, \theta) = (1, 2)$ position. Using the expressions for the derivatives of unit vectors we find that the derivatives now include those of the tensor elements (e.g., $\tau_{\phi\theta}$), as well as the derivatives of both unit vectors multiplying each tensor element. We therefore expect two correction terms due to the derivatives of the unit vectors, rather than just one in the case of the divergence of a vector. This

leads to the additional terms in the momentum equation discussed in the text.

References

Abbot, D. S., and R. T. Pierrehumbert (2010), Mudball: Surface dust and Snowball Earth deglaciation, *J. Geophys. Res.*, *115*, D03104, doi:10.1029/2009JD012007.

Abbot, D. S., A. Voigt, and D. Koll (2011), The Jormungand global climate state and implications for Neoproterozoic Glaciations, *J. Geophys. Res.*, *116*, D18103, doi:10.1029/2011JD015927.

Adcroft, A., J. Campin, C. Hill, and J. Marshall (2004), Implementation of an atmosphere-ocean general circulation model on the expanded spherical cube, *Mon. Weath. Rev.*, *132*(12), 2845–2863, doi:10.1175/MWR2823.1.

Campbell, A. J., E. D. Waddington, and S. G. Warren (2011), Refugium for surface life on Snowball Earth in a nearly-enclosed sea? A first simple model for sea-glacier invasion, *Geophys. Res. Lett.*, *38*, L19502, doi:10.1029/2011GL048846.

Chandler, M., and L. Sohl (2000), Climate forcings and the initiation of low-latitude ice sheets during the Neoproterozoic Varanger glacial interval, *J. Geophys. Res.*, *105*(D16), 20,737–20,756.

Doake, C., and D. Vaughan (1991), Rapid disintegration of the Wordie Ice Shelf in response to atmospheric warming, *Nature*, *350*(6316), 328–330, doi:10.1038/350328a0.

Doake, C., H. Corr, H. Rott, P. Skvarca, and N. Young (1998), Breakup and conditions for stability of the northern Larsen Ice Shelf, Antarctica, *Nature*, *391*(6669), 778–780, doi:10.1038/35832.

Glen, J. (1955), The creep of polycrystalline ice, *Proc. R. Soc. London, Ser. A*, *228*(1175), 519–538, doi:10.1098/rspa.1955.0066.

Goodman, J. C. (2006), Through thick and thin: Marine and meteoric ice in a "Snowball Earth" climate, *Geophys. Res. Lett.*, *33*, L16701, doi:10.1029/2006GL026840.

Goodman, J. C., and R. T. Pierrehumbert (2003), Glacial flow of floating marine ice in "Snowball Earth", *J. Geophys. Res.*, *108*(C10), 3308, doi:10.1029/2002JC001471.

Greenberg, M. (1998), *Advanced Engineering Mathematics*, 2nd ed., 1324 pp., Prentice Hall, Upper Saddle River, N. J.

Harland, W. B. (1964), Evidence of late Precambrian glaciation and its significance, in *Problems in Palaeoclimatology*, edited by A. E. M. Nairn, pp. 119–149, John Wiley, London.

Hoffman, P. F., and D. P. Schrag (2002), The snowball Earth hypothesis: Testing the limits of global change, *Terra Nova*, *14*(3), 129–155, doi:10.1046/j.1365-3121.2002.00408.x.

Hoffman, P. F., A. J. Kaufman, G. P. Halverson, and D. P. Schrag (1998), A Neoproterozoic snowball Earth, *Science*, *281*(5381), 1342–1346.

Hyde, W. T., T. J. Crowley, S. K. Baum, and W. R. Peltier (2000), Neoproterozoic 'snowball earth' simulations with a coupled climate/ice-sheet model, *Nature*, *405*, 425–429.

Kirschvink, J. (1992), Late Proterozoic low-latitude global glaciation: The Snowball Earth, in *The Proterozoic Biosphere: A Multidisciplinary Study*, edited by J. Schopf and C. Klein, pp. 51–52, Cambridge Univ. Press, Cambridge, U. K.

Le Hir, G., Y. Donnadieu, G. Krinner, and G. Ramstein (2010), Toward the snowball Earth deglaciation…, *Clim. Dyn.*, *35*(2–3), 285–297, doi:10.1007/s00382-010-0748-8.

Lewis, J. P., A. J. Weaver, and M. Eby (2007), Snowball versus slushball Earth: Dynamic versus nondynamic sea ice?, *J. Geophys. Res.*, *112*, C11014, doi:10.1029/2006JC004037.

Li, D., and R. T. Pierrehumbert (2011), Sea glacier flow and dust transport on snowball Earth, *Geophys. Res. Lett.*, *38*, L17501, doi:10.1029/2011GL048991.

Li, Z. X., et al. (2008), Assembly, configuration, and break-up history of Rodinia: A synthesis, *Precambrian Res.*, *160*, 179–210.

Liu, Y., and W. R. Peltier (2010), A carbon cycle coupled climate model of Neoproterozoic glaciation: Influence of continental configuration on the formation of a "soft snowball", *J. Geophys. Res.*, *115*, D17111, doi:10.1029/2009JD013082.

MacAyeal, D. (1989), Large-scale ice flow over a viscous basal sediment: Theory and application to ice stream B, Antarctica, *J. Geophys. Res.*, *94*(B4), 4071–4087.

MacAyeal, D. (1997), Eismint: Lessons in ice-sheet modeling, technical report, Univ. of Chicago, Chicago, Ill.

MacAyeal, D., and V. Barcilon (1988), Ice-shelf response to ice-stream discharge fluctuations. 1. Unconfined ice tongues, *J. Glaciol.*, *34*(116), 121–127.

MacAyeal, D., T. Scambos, C. Hulbe, and M. Fahnestock (2003), Catastrophic ice-shelf break-up by an ice-shelf-fragment-capsize mechanism, *J. Glaciol.*, *49*(164), 22–36.

McKay, C. (2000), Thickness of tropical ice and photosynthesis on a snowball Earth, *Geophys. Res. Lett.*, *27*(14), 2153–2156, doi:10.1029/2000GL008525.

Morland, L. (1987), Unconfined ice-shelf flow, in *Dynamics of the West Antarctic Ice Sheet*, edited by C. van der Veen and J. Oerlemans, pp. 99–116, D. Reidel, Boston, Mass.

Nye, J. F. (1965), The flow of a glacier in a channel of rectangular, elliptical or parabolic cross-section, *J. Glaciol.*, *5*(41), 661–690.

Pierrehumbert, R. T., D. S. Abbot, A. Voigt, and D. Koll (2011), Climate of the Neoproterozoic, *Annu. Rev. Earth Planet. Sci.*, *39*, 417–460.

Pollard, D., and J. Kasting (2005), Snowball Earth: A thin-ice solution with flowing sea glaciers, *J. Geophys. Res.*, *110*, C07010, doi:10.1029/2004JC002525.

Pollard, D., and J. F. Kasting (2006), Reply to comment by Stephen G. Warren and Richard E. Brandt on "Snowball Earth: A thin-ice solution with flowing sea glaciers", *J. Geophys. Res.*, *111*, C09017, doi:10.1029/2006JC003488.

Rott, H., P. Skvarca, and T. Nagler (1996), Rapid collapse of northern Larsen Ice Shelf, Antarctica, *Science*, *271*(5250), 788–792, doi:10.1126/science.271.5250.788.

Schoof, C. (2006), A variational approach to ice stream flow, *J. Fluid Mech.*, *556*, 227–251, doi:10.1017/S0022112006009591.

van der Veen, C. (1999), *Fundamentals of Glacier Dynamics*, A. A. Balkema, Rotterdam, Netherlands.

Vieli, A., A. J. Payne, Z. Du, and A. Shepherd (2006), Numerical modelling and data assimilation of the Larsen B ice shelf, Antarctic Ppeninsula, *Philos. Trans. R. Soc. A*, *364*(1844), 1815–1839, doi:10.1098/rsta.2006.1800.

Voigt, A., D. S. Abbot, R. T. Pierrehumbert, and J. Marotzke (2011), Initiation of a Marinoan Snowball Earth in a state-of-the-art atmosphere-ocean general circulation model, *Clim. Past*, *7*, 249–263, doi:10.5194/cp-7-249-2011.

Warren, S. G., and R. E. Brandt (2006), Comment on "Snowball Earth: A thin-ice solution with flowing sea glaciers" by David Pollard and James F. Kasting, *J. Geophys. Res.*, *111*, C09016, doi:10.1029/2005JC003411.

Warren, S. G., R. E. Brandt, T. C. Grenfell, and C. P. McKay (2002), Snowball Earth: Ice thickness on the tropical ocean, *J. Geophys. Res.*, *107*(C10), 3167, doi:10.1029/2001JC001123.

Weertman, J. (1957), Deformation of floating ice shelves, *J. Glaciol.*, *3*(21), 38–42.

Weis, M., R. Greve, and K. Hutter (1999), Theory of shallow ice shelves, *Continuum Mech. Thermodyn.*, *11*(1), 15–50, doi:10.1007/s001610050102.

Informal supplementary for: Continental constriction and oceanic ice-cover thickness in a Snowball-Earth scenario: finite difference formulation

Eli Tziperman,[1] Dorian S. Abbot,[2] Yosef Ashkenazy,[3] Hezi Gildor,[4]

David Pollard,[5] Christian G. Schoof,[6] and Daniel P. Schrag[1]

4   **Abstract.**   This SI contains the finite difference formulation of the ice flow

5   model.

――――――

Eli Tziperman, Department of Earth and Planetary Sciences and School of engineer-

ing and applied sciences, Harvard University, 20 Oxford St, Cambridge, MA, 02138, USA.

(eli@eps.harvard.edu)

Dorian Schuyler Abbot, Department of Geophysical Sciences, University of Chicago, 5734

South Ellis Avenue, Chicago, IL 60637, USA. (Abbot@uchicago.edu)

Yosef Ashkenazy, Department of Solar Energy and Environmental Physics, BIDR, Ben-Gurion

University, Midreshet Ben-Gurion, 84990, Israel. (ashkena@bgu.ac.il)

Hezi Gildor, The Fredy and Nadine Herrmann Institute of Earth Sciences, The Hebrew Uni-

versity of Jerusalem, Jerusalem, 91904, Israel. (Hezi.Gildor@huji.ac.il)

David Pollard, Department of Geosciences, Earth and Environmental Systems Institute, Penn-

sylvania State University, University Park, PA 16802, USA. (pollard@essc.psu.edu)

Christian Schoof, Department of Earth and Ocean Sciences, University of British Columbia,

6339 Stores Road, Vancouver, British Columbia Canada, V6T 1Z4. (cschoof@eos.ubc.ca)

Dan Schrag, Department of Earth and Planetary Sciences, Harvard University, 20 Oxford St,

Cambridge, MA, 02138, USA. (schrag@eps.harvard.edu)

[1]Department of Earth and Planetary

1. Finite difference formulation in spherical coordinates

sciences and school of engineering and

applied sciences, Cambridge, MA, USA.

[2]Department of Geophysical Sciences at

the University of Chicago, Chicago, IL,

USA.

[3]Department of Solar Energy and

Environmental Physics, BIDR, Ben-Gurion

University, Midreshet Ben-Gurion, Israel.

[4]The Fredy and Nadine Herrmann

Institute of Earth Sciences, The Hebrew

University of Jerusalem, Jerusalem, Israel.

[5]Department of Geosciences, Earth and

Environmental Systems Institute,

Pennsylvania State University, University

Park, PA, USA.

[6]Department of Earth and Ocean

Sciences, University of British Columbia,

Vancouver, British Columbia, Canada.

1.1. 1d

$$0 = \left[\frac{1}{\sin\theta}\partial_\theta\left(B\sin\theta\partial_\theta v\right) + \partial_\theta\left(B\frac{1}{\sin\theta}\partial_\theta(v\sin\theta)\right)\right.$$

$$\left. - B\cot^2\theta v\right] - g\rho_I(1-\mu)hh_\theta$$

$$B = \frac{1}{r}h\langle A(T)^{-\frac{1}{3}}\rangle\dot{\epsilon}^{\frac{1}{3}-1}$$

$$\dot{\epsilon}^2 = \dot{\epsilon}_{\phi\phi}^2 + \dot{\epsilon}_{\theta\theta}^2 + \dot{\epsilon}_{zz}^2$$

$$\dot{\epsilon}_{zz} = -(\dot{\epsilon}_{\theta\theta} + \dot{\epsilon}_{\phi\phi})$$

$$h_t + \frac{1}{r\sin\theta}\partial_\theta(\sin\theta vh) = \kappa\nabla^2 h + S(\theta).$$

is written in finite difference as

$$s_j^{-1}\left(B_{j+\frac{1}{2}}s_{j+\frac{1}{2}}(v_{j+1} - v_j) - B_{j-\frac{1}{2}}s_{j-\frac{1}{2}}(v_j - v_{j-1})\right)/d\theta^2$$

$$+ \left(B_{j+\frac{1}{2}}s_{j+\frac{1}{2}}^{-1}(v_{j+1}s_{j+1} - v_js_j) - B_{j-\frac{1}{2}}s_{j-\frac{1}{2}}^{-1}(v_js_j - v_{j-1}s_{j-1})\right)/d\theta^2$$

$$- \cot\theta_j B_j s_j^{-1}v_j\cos\theta_j$$

$$= g\rho_I(1-\mu)h_j(h_{j+1} - h_{j-1})/(2d\theta)$$

which may be written in a tri-diagonal form,

$$v_{j+1}\left[s_j^{-1}B_{j+\frac{1}{2}}s_{j+\frac{1}{2}}/d\theta^2 + B_{j+\frac{1}{2}}s_{j+\frac{1}{2}}^{-1}s_{j+1}/d\theta^2\right]$$

$$+ v_j\left[-s_j^{-1}B_{j+\frac{1}{2}}s_{j+\frac{1}{2}}/d\theta^2 - B_{j+\frac{1}{2}}s_{j+\frac{1}{2}}^{-1}s_j/d\theta^2) - B_{j-\frac{1}{2}}s_{j-\frac{1}{2}}^{-1}s_j/d\theta^2 - s_j^{-1}B_{j-\frac{1}{2}}s_{j-\frac{1}{2}}/d\theta^2\right.$$

$$\left. - \cot\theta_j B_j s_j^{-1}\cos\theta_j\right]$$

$$+ v_{j-1}\left[s_j^{-1}B_{j-\frac{1}{2}}s_{j-\frac{1}{2}}/d\theta^2 + B_{j-\frac{1}{2}}s_{j-\frac{1}{2}}^{-1}s_{j-1}/d\theta^2)\right]$$

$$= g\rho_I(1-\mu)h_j(h_{j+1} - h_{j-1})/(2d\theta)$$

1.2. 2d

With

$$B_{ij} = \frac{1}{r}h_{ij}\langle A^{-\frac{1}{3}}\rangle\dot{\epsilon}^{\frac{1}{3}-1}$$

$$s_j = \sin\theta_j$$

$$c_j = \cos\theta_j$$

the above equations become,

$$0 = -g\rho_I h_{ij}(1-\mu)(h_{i+1,j} - h_{i-1,j})/(2d\phi) \tag{3}$$

$$+ \left(2B_{i+\frac{1}{2},j}\frac{1}{s_j}(u_{i+1,j} - u_{i,j}) - 2B_{i-\frac{1}{2},j}\frac{1}{s_j}(u_{i,j} - u_{i-1,j})\right)/d\phi^2$$

$$+2\frac{c_j}{s_j}\left(B_{i+1,j}v_{i+1,j} - B_{i-1,j}v_{i-1,j}\right)/(2d\phi)$$

$$+ \left(B_{i+1,j}(v_{i+1,j+1} - v_{i+1,j-1}) - B_{i-1,j}(v_{i-1,j+1} - v_{i-1,j-1})\right)/(4d\phi\,d\theta)$$

$$+ \frac{1}{2}\left(B_{i,j+1}(v_{i+1,j+1} - v_{i-1,j+1}) - B_{i,j-1}(v_{i+1,j-1} - v_{i-1,j-1})\right)/(4d\phi\,d\theta)$$

$$+ \frac{1}{2}\left(s_{j+\frac{1}{2}}^2 B_{i,j+\frac{1}{2}}(u_{i,j+1}/s_{j+1} - u_{i,j}/s_j) - s_{j-\frac{1}{2}}^2 B_{i,j-\frac{1}{2}}(u_{i,j}/s_j - u_{i,j-1}/s_{j-1})\right)/d\theta^2$$

$$+ \cot\theta_j B_{i,j}\frac{1}{2}\left((v_{i+1,j} - v_{i-1,j})/(2d\phi) + s_j^2(u_{i,j+1}/s_{j+1} - u_{i,j-1}/s_{j-1})/(2d\theta)\right)$$

$$0 = -s_j g\rho_I h_{ij}(1-\mu)(h_{i,j+1} - h_{i,j-1})/(2d\theta)$$

$$+ \frac{1}{s_j}\frac{1}{2}\left(B_{i+\frac{1}{2},j}(v_{i+1,j} - v_{i,j}) - B_{i-\frac{1}{2},j}(v_{i,j} - v_{i-1,j})\right)/d\phi^2$$

$$+ \frac{1}{2}\left(B_{i+1,j}s_j(u_{i+1,j+1}/s_{j+1} - u_{i+1,j-1}/s_{j-1}) - B_{i-1,j}s_j(u_{i-1,j+1}/s_{j+1} - u_{i-1,j-1}/s_{j-1})\right)/(4d\phi\,d\theta)$$

$$+ \left(B_{i,j+\frac{1}{2}}s_{j+\frac{1}{2}}(v_{i,j+1} - v_{i,j}) - B_{i,j-\frac{1}{2}}s_{j-\frac{1}{2}}(v_{i,j} - v_{i,j-1})\right)/d\theta^2$$

$$+s_j\left(B_{i,j+\frac{1}{2}}\frac{1}{s_{j+\frac{1}{2}}}(v_{i,j+1}s_{j+1} - v_{i,j}s_j) - B_{i,j-\frac{1}{2}}\frac{1}{s_{j-\frac{1}{2}}}(v_{i,j}s_j - v_{i,j-1}s_{j-1})\right)/d\theta^2$$

$$+ s_j\left(B_{i,j+1}\frac{1}{s_{j+1}}(u_{i+1,j+1} - u_{i-1,j+1}) - B_{i,j-1}\frac{1}{s_{j-1}}(u_{i+1,j-1} - u_{i-1,j-1})\right)/(4d\phi\,d\theta)$$

$$- \cot\theta_j B_{i,j}\left((u_{i+1,j} - u_{i-1,j})/(2d\phi) + c_j v_{i,j}\right)$$

$$\partial_t h_{ij} + \left(h_{i+1,j}u_{i+1,j} - h_{i-1,j}u_{i-1,j}\right)/(2d\phi) + \left(h_{i,j+1}v_{i,j+1} - h_{i,j-1}v_{i,j-1}\right)/(2d\theta)$$

$$= \hat{\kappa}\left((h_{i+1,j} - 2h_{i,j} + h_{i-1,j})/d\phi^2 + (h_{i,j+1} - 2h_{i,j} + h_{i,j-1})/d\theta^2\right) + S_{ij}.$$

49 To solve the momentum equations using a matrix solver, we need to write them as follows

50 $$g\rho_I h_{ij}(1-\mu)(h_{i+1,j}-h_{i-1,j})/(2d\phi) =$$

51 $$+ u_{i-1,j-1}\,()$$

52 $$+ u_{i,j-1}\left(\frac{1}{2}B_{i,j-\frac{1}{2}}\frac{s_{j-\frac{1}{2}}^2}{s_{j-1}}/d\theta^2 - \cot\theta_j B_{i,j}\frac{1}{2}s_j^2/(s_{j-1}2d\theta)\right)$$

53 $$+ u_{i+1,j-1}\,()$$

54 $$+ u_{i-1,j}\left(2B_{i-\frac{1}{2},j}\frac{1}{s_j}/d\phi^2\right)$$

55 $$+ u_{i,j}\left(-2B_{i+\frac{1}{2},j}\frac{1}{s_j}/d\phi^2 - 2B_{i-\frac{1}{2},j}\frac{1}{s_j}/d\phi^2 - \frac{1}{2}B_{i,j+\frac{1}{2}}\frac{s_{j+\frac{1}{2}}^2}{s_j}/d\theta^2 - \frac{1}{2}B_{i,j-\frac{1}{2}}\frac{s_{j-\frac{1}{2}}^2}{s_j}/d\theta^2\right)$$

56 $$+ u_{i+1,j}\left(2B_{i+\frac{1}{2},j}\frac{1}{s_j}/d\phi^2\right)$$

57 $$+ u_{i-1,j+1}\,()$$

58 $$+ u_{i,j+1}\left(\frac{s_{j+\frac{1}{2}}^2}{s_{j+1}}\frac{1}{2}B_{i,j+\frac{1}{2}}/d\theta^2 + \cot\theta_j B_{i,j}\frac{1}{2}s_j^2/(s_{j+1}2d\theta)\right)$$

59 $$+ u_{i+1,j+1}\,()$$

60 $$+ v_{i-1,j-1}\left(\frac{1}{2}B_{i,j-1}/(4d\phi\,d\theta) + B_{i-1,j}/(4d\phi\,d\theta)\right)$$

61 $$+ v_{i,j-1}\,()$$

62 $$+ v_{i+1,j-1}\left(-\frac{1}{2}B_{i,j-1}/(4d\phi\,d\theta) - B_{i+1,j}/(4d\phi\,d\theta)\right)$$

63 $$+ v_{i-1,j}\left(-2\frac{c_j}{s_j}B_{i-1,j}/(2d\phi) - \cot\theta_j B_{i,j}\frac{1}{2}/(2d\phi)\right)$$

64 $$+ v_{i,j}\,()$$

65 $$+ v_{i+1,j}\left(+2\frac{c_j}{s_j}B_{i+1,j}/(2d\phi) + \cot\theta_j B_{i,j}\frac{1}{2}/(2d\phi)\right)$$

66 $$+ v_{i-1,j+1}\left(-\frac{1}{2}B_{i,j+1}/(4d\phi\,d\theta) - B_{i-1,j}/(4d\phi\,d\theta)\right)$$

67 $$+ v_{i,j+1}\,()$$

68 $$+ v_{i+1,j+1}\left(\frac{1}{2}B_{i,j+1}/(4d\phi\,d\theta) + B_{i+1,j}/(4d\phi\,d\theta)\right)$$

69

70   and

71   $s_j g \rho_I h_{ij}(1-\mu)(h_{i,j+1} - h_{i,j-1})/(2d\theta) =$

72   $+ u_{i-1,j-1}\left(\dfrac{1}{2}B_{i-1,j}\dfrac{s_j}{s_{j-1}}/(4d\phi\,d\theta) + s_j B_{i,j-1}\dfrac{1}{s_{j-1}}/(4d\phi\,d\theta)\right)$

73   $+ u_{i,j-1}\,()$

74   $+ u_{i+1,j-1}\left(-\dfrac{1}{2}B_{i+1,j}\dfrac{s_j}{s_{j-1}}/(4d\phi\,d\theta) - s_j B_{i,j-1}\dfrac{1}{s_{j-1}}/(4d\phi\,d\theta)\right)$

75   $+ u_{i-1,j}\left(+\cot\theta_j B_{i,j}/(2d\phi)\right)$

76   $+ u_{i,j}\,()$

77   $+ u_{i+1,j}\left(-\cot\theta_j B_{i,j}/(2d\phi)\right)$

78   $+ u_{i-1,j+1}\left(-\dfrac{1}{2}B_{i-1,j}\dfrac{s_j}{s_{j+1}}/(4d\phi\,d\theta) - s_j B_{i,j+1}\dfrac{1}{s_{j+1}}/(4d\phi\,d\theta)\right)$

79   $+ u_{i,j+1}\,()$

80   $+ u_{i+1,j+1}\left(\dfrac{1}{2}B_{i+1,j}\dfrac{s_j}{s_{j+1}}/(4d\phi\,d\theta) + s_j B_{i,j+1}\dfrac{1}{s_{j+1}}/(4d\phi\,d\theta)\right)$

81   $+ v_{i-1,j-1}\,()$

82   $+ v_{i,j-1}\left(B_{i,j-\frac{1}{2}}s_{j-\frac{1}{2}}/d\theta^2 + s_j B_{i,j-\frac{1}{2}}\dfrac{1}{s_{j-\frac{1}{2}}}s_{j-1}/d\theta^2\right)$

83   $+ v_{i+1,j-1}\,()$

84   $+ v_{i-1,j}\left(\dfrac{1}{2}B_{i-\frac{1}{2},j}\dfrac{1}{s_j}/d\phi^2\right)$

85   $+ v_{i,j}\left(-\dfrac{1}{2}B_{i+\frac{1}{2},j}\dfrac{1}{s_j}/d\phi^2 - \dfrac{1}{2}B_{i-\frac{1}{2},j}\dfrac{1}{s_j}/d\phi^2 - B_{i,j+\frac{1}{2}}s_{j+\frac{1}{2}}/d\theta^2 - B_{i,j-\frac{1}{2}}s_{j-\frac{1}{2}}/d\theta^2\right.$

86   $-s_j^2 B_{i,j-\frac{1}{2}}\dfrac{1}{s_{j-\frac{1}{2}}}/d\theta^2 - s_j^2 B_{i,j+\frac{1}{2}}\dfrac{1}{s_{j+\frac{1}{2}}}/d\theta^2$

87   $\left. -\cot\theta_j B_{i,j}c_j\right)$

88   $+ v_{i+1,j}\left(\dfrac{1}{2}B_{i+\frac{1}{2},j}\dfrac{1}{s_j}/d\phi^2\right)$

89   $+ v_{i-1,j+1}\,()$

90   $+ v_{i,j+1}\left(B_{i,j+\frac{1}{2}}s_{j+\frac{1}{2}}/d\theta^2 + s_j B_{i,j+\frac{1}{2}}\dfrac{1}{s_{j+\frac{1}{2}}}s_{j+1}/d\theta^2\right)$

91
92   $+ v_{i+1,j+1}\,()$